Nigerian Journal of Applied Physics (NJAP)
ISSN Print: 3115-5871
ISSN Online: 3115-588X
DOI: https://doi.org/10.62292/njap-v2i2-2026-93
Volume 2(2), June 2026

Influence of ZnSe Donor Doping and Resistive Parameters on the Photovoltaic Performance of an $MASnI_3$ Perovskite Solar Cell: A SCAPS-1D Numerical Study

***Samuel O. Adeosun, Joshua A. Owolabi, Ijeoma N. Ukorah, Rapheal U. Ugbe and Rabiu A. Tafida**

Department of Physics, Faculty of Science, Nigerian Defence Academy, Kaduna State, Nigeria.

*Corresponding author's email: adeosuns51@gmail.com

ABSTRACT

Perovskite solar cells are promising next-generation photovoltaic devices, but their performance is strongly influenced by charge-transport losses and parasitic resistive effects. This study numerically investigates the influence of ZnSe donor concentration, series resistance (Rs), and shunt resistance (Rsh) on an FTO/ZnSe/$MASnI_3$/Graphene/Au perovskite solar cell using SCAPS-1D. Simulations were performed under AM1.5G illumination of 1000 W m^{-2} at 300 K. The ZnSe donor concentration was varied from 10^{15} to 10^{22} cm^{-3}, while Rs was varied from 0.2 to 1.6 Ω cm^2 and Rsh from 2000 to 3400 Ω cm^2. The optimum baseline performance occurred at a ZnSe donor concentration of 10^{17} cm^{-3}, yielding Voc = 1.139 V, Jsc = 27.215 mA cm^{-2}, FF = 88.675%, and PCE = 27.486%. At 10^{19} cm^{-3}, PCE decreased sharply to 21.586%, indicating the adverse effect of excessive doping. Increasing Rs from 0.2 to 1.6 Ω cm^2 reduced FF from 88.222% to 85.060% and PCE from 27.346% to 26.367%, while Voc and Jsc changed only marginally. Increasing Rsh from 2000 to 3400 Ω cm^2 increased FF from 86.991% to 87.684% and PCE from 26.948% to 27.170%. The integrated optimized configuration reported in the MSc study achieved Jsc = 30.89 mA cm^{-2}, Voc = 1.23 V, FF = 78.29%, and PCE = 29.70%. The results show that controlled ZnSe doping, low series resistance and sufficiently high shunt resistance are important for minimizing electrical losses and improving charge extraction.

Keywords:
ZnSe,
$MASnI_3$,
Perovskite Solar Cell,
SCAPS-1D,
Series Resistance.

INTRODUCTION

Perovskite solar cells (PSCs) have attracted extensive research interest because of their strong optical absorption, tunable electronic properties and potential for high photovoltaic efficiency. The rapid development of perovskite absorbers and selective transport layers has made PSCs an important class of emerging thin-film photovoltaic devices (Jena et al., 2019; Lin, 2020). Charge-selective layers are particularly important because they determine carrier extraction, transport, interfacial recombination, and the resistive losses that ultimately shape the current-voltage characteristics.

Zinc selenide (ZnSe) is a wide-bandgap semiconductor that has been investigated as an electron transport material (ETM) for planar PSCs. Its electronic properties and suitable band alignment can support electron extraction while reducing undesirable carrier accumulation at the absorber/ETM interface. Numerical and experimental studies have demonstrated the potential of ZnSe-based transport structures for improving PSC performance (Li et al., 2018; Li et al., 2023; Owolabi et al., 2020; Ukorah et al., 2024).

The donor concentration of an ETM is an important parameter because it controls free-carrier density and electrical conductivity. Increasing donor concentration can improve electron transport and strengthen internal electric fields, but excessive doping may introduce enhanced recombination, scattering, and non-ideal electrostatic behaviour. Hima et al. (2017) and Tailor et al. (2023) emphasized the importance of optimizing transport-layer doping rather than simply maximizing the dopant concentration.

Parasitic resistance is another important limitation. Series resistance represents resistive losses along the current path and is especially detrimental around the maximum power point, where both current and voltage are significant. Experimental and theoretical investigations have shown that increasing series resistance can substantially reduce fill factor and efficiency (Wu et al., 2014; Kirchartz et al., 2018; Mundhaas et al., 2019). Shunt resistance describes unwanted parallel leakage pathways. Low shunt resistance causes photogenerated carriers to bypass the useful external circuit, reducing the fill factor and power output; consequently, high shunt resistance is generally desirable (Kirchartz et al., 2020; Tvingstedt et al., 2017).

The present work focuses specifically on the third and fourth objectives of the completed MSc study: evaluating the influence of ZnSe donor concentration on the photovoltaic characteristics of the proposed device and optimizing the resistive parameters Rs and Rsh. The analysis provides a quantitative assessment of how these parameters affect Voc, Jsc, FF and PCE in the FTO/ZnSe/$MASnI_3$/Graphene/Au architecture.

MATERIALS AND METHODS

The proposed planar device architecture was FTO/ZnSe/$MASnI_3$/Graphene/Au, where FTO served as the front transparent electrode, ZnSe as the ETM, $MASnI_3$ as the absorber, graphene as the hole transport material (HTM), and Au as the rear contact. The layer sequence and material parameters were taken directly from the completed MSc simulation study.

Table 1: Principal Material Parameters used in the SCAPS-1D Model

Parameter	FTO	ZnSe	$MASnI_3$	Graphene
Thickness (μm)	0.400	0.100	1.100	0.020
Bandgap (eV)	3.500	2.900	1.300	0.900
Electron affinity (eV)	4.000	4.090	4.170	4.500
Relative permittivity	9.0	10.0	8.2	4.0
Electron mobility ($cm^2 V^{-1} s^{-1}$)	20	50	1.6	10
Hole mobility ($cm^2 V^{-1} s^{-1}$)	10	20	1.6	200
Baseline donor density (cm^{-3})	—	1×10^{17}	0	0
Acceptor density (cm^{-3})	0	0	1×10^{16}	1×10^{16}

The numerical simulations were carried out in SCAPS-1D under standard AM1.5G illumination at 1000 W m^{-2} and a temperature of 300 K, with ohmic front and back contacts. Bulk and interface defect states were included in the model. The absorber bulk defect density and interface defect densities were retained at the optimized values established in the preceding stages of the MSc study, while the parameters associated with Objectives 3 and 4 were varied.

For the ZnSe doping study, the donor concentration was varied from 10^{15} to 10^{22} cm^{-3}. For each concentration, the simulated current-voltage response and the photovoltaic parameters Voc, Jsc, FF, and PCE were recorded. The isolated parameter sweeps for series and shunt resistance were then performed over Rs = 0.2–1.6 Ω cm^2 and Rsh = 2000–3400 Ω cm^2, respectively.

Power conversion efficiency was evaluated from the standard photovoltaic relationship PCE = Voc × Jsc × FF / Pin, with consistent units for the electrical quantities and Pin = 1000 W m^{-2}. The analysis focused on identifying parameter ranges that maximize useful charge extraction while minimizing resistive losses.

RESULTS AND DISCUSSION

Influence of ZnSe Donor Concentration

The ZnSe donor concentration strongly influenced the photovoltaic characteristics of the simulated cell. Table 2 shows the complete sweep obtained from the MSc simulation. The PCE increased from 25.760% at 10^{15} cm^{-3} to 27.486% at 10^{17} cm^{-3}. Over the same range, FF increased from 83.110% to 88.675%, indicating improved diode quality and charge extraction. The optimum baseline point was therefore 10^{17} cm^{-3}.

Table 2: Effect of ZnSe Donor Concentration on the Photovoltaic Parameters

ZnSe donor concentration (cm^{-3})	Voc (V)	Jsc (mA cm^{-2})	FF (%)	PCE (%)
1×10^{15}	1.141296	27.15815	83.11026	25.76043
1×10^{16}	1.141020	27.16527	84.98653	26.34252
1×10^{17}	1.138977	27.21451	88.67541	27.48644
1×10^{18}	1.125355	27.35232	88.27862	27.17309
1×10^{19}	0.971118	27.55883	80.65626	21.58594
1×10^{20}	1.136503	27.65686	87.28985	27.43705
1×10^{21}	1.139791	27.62411	87.22397	27.46309

ZnSe donor concentration (cm^{-3})	Voc (V)	Jsc (mA cm^{-2})	FF (%)	PCE (%)
1×10^{22}	1.139979	27.59350	87.21702	27.43500

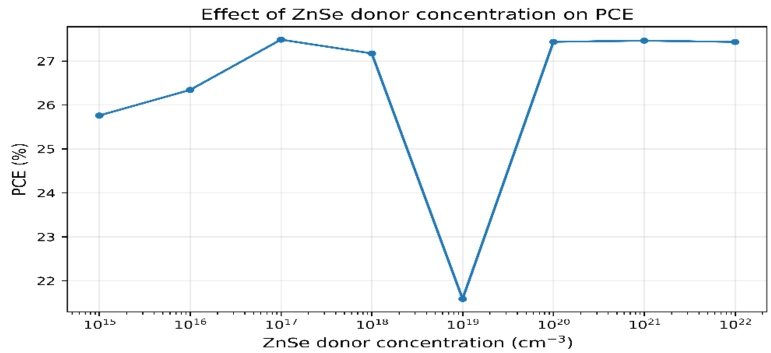

Figure 1: Variation of PCE with ZnSe donor concentration

The initial increase in efficiency is consistent with improved electron transport as donor concentration is raised from 10^{15} to 10^{17} cm^{-3}. The improvement in FF is particularly important because it indicates a more favourable current-voltage response. The simulation therefore suggests that moderate donor doping provides a useful balance between conductivity, carrier extraction and recombination.

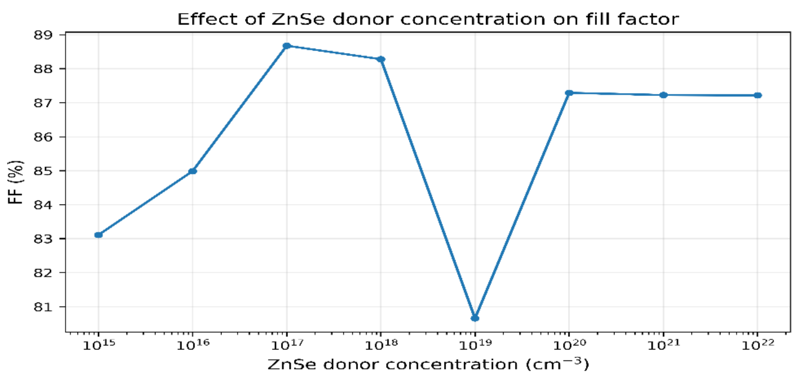

Figure 2: Variation of fill factor with ZnSe donor concentration.

At 10^{19} cm^{-3}, the device exhibits a pronounced degradation: Voc falls to 0.971 V, FF falls to 80.656%, and PCE decreases to 21.586%. The MSc study attributes this deterioration to excessive recombination, impurity scattering and deterioration of diode quality. At still higher concentrations, the simulated PCE and FF partially recover. Because this recovery occurs at extremely high donor densities, it should be treated cautiously rather than interpreted as a practical optimum; the thesis itself notes possible degenerate-doping, band-structure and numerical-convergence effects at such concentrations.

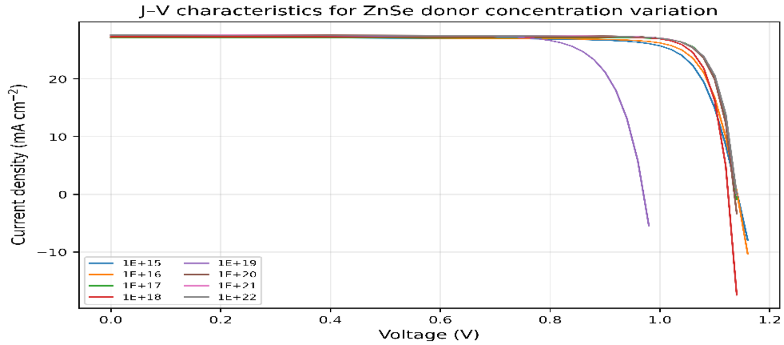

Figure 3: Simulated J–V characteristics for the ZnSe donor concentration sweep

The J–V curves further show that moderate doping maintains a well-behaved diode response, whereas the high-doping cases become increasingly non-ideal. The Jsc response is comparatively weak over the lower doping range, increasing from 27.158 to 27.215 mA cm^{-2} between 10^{15} and 10^{17} cm^{-3}. The current rises further at higher concentrations, reaching 27.657 mA cm^{-2} at 10^{20} cm^{-3}, but this does not translate into higher PCE because Voc and FF deteriorate at critical doping levels.

An important limitation of the present analysis is that the MSc study does not report an independently extracted numerical Rs value for every ZnSe donor concentration. Consequently, the effect of doping on resistive transport is interpreted from the J–V and photovoltaic-parameter response rather than presented as a direct measured or separately simulated Rs-versus-doping relationship.

The present ZnSe donor-concentration results are broadly consistent with previous studies emphasizing the importance of optimizing rather than simply maximizing the doping level of charge-transport layers. Hima et al. (2017) demonstrated through SCAPS-1D simulations that doping concentration can significantly influence the photovoltaic response of perovskite solar cells, supporting the need for an optimized carrier concentration. Similarly, Tailor et al. (2023) emphasized that controlled doping is important for regulating charge transport and recombination in perovskite photovoltaic devices. The present study further demonstrates this behaviour for ZnSe used as the electron transport material in the FTO/ZnSe/$MASnI_3$/Graphene/Au structure, with the optimum baseline performance obtained at a donor concentration of 10^{17} cm^{-3}. This result is also consistent with the reported potential of ZnSe as an electron-transport layer in perovskite solar cells (Li et al., 2018; Li et al., 2023; Owolabi et al., 2020). In addition, the use of $MASnI_3$ with ZnSe and graphene is related to the structure investigated by Ukorah et al. (2024), although the present work focuses specifically on the combined influence of ZnSe donor concentration, series resistance, and shunt resistance. The pronounced reduction in performance at 10^{19} cm^{-3} observed in the present simulation further indicates that excessive donor concentration can be detrimental to device performance, reinforcing the general conclusion from previous studies that transport-layer doping must be carefully optimized.

Effect of Series Resistance

The isolated series-resistance sweep is summarized in Table 3. Increasing Rs from 0.2 to 1.6 Ω cm² produced only negligible changes in Voc and Jsc, but caused a systematic decline in FF and PCE.

Table 3. Effect of Series Resistance on the Photovoltaic Parameters

Rs (Ω cm²)	Voc (V)	Jsc (mA cm^{-2})	FF (%)	PCE (%)
0.2	1.139000	27.21426	88.22244	27.34634
0.4	1.139021	27.21401	87.76982	27.20629
0.6	1.139040	27.21376	87.31752	27.06630
0.8	1.139057	27.21351	86.86553	26.92635
1.0	1.139073	27.21326	86.41383	26.78647
1.2	1.139088	27.21301	85.96241	26.64663
1.4	1.139101	27.21276	85.51126	26.50686
1.6	1.139114	27.21251	85.06037	26.36713

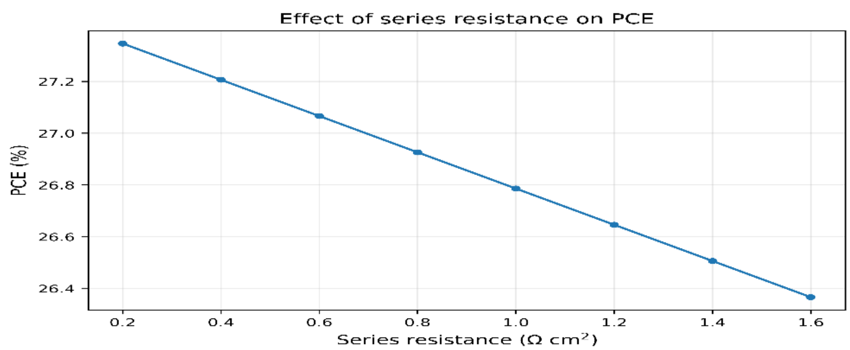

Figure 4: Effect of series resistance on PCE.

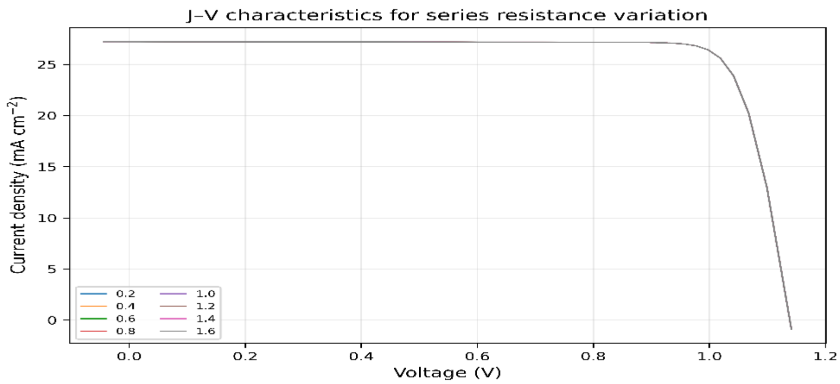

Figure 5: Simulated J–V characteristics for different series-resistance values.

The PCE decreases from 27.346% to 26.367% as Rs increases across the investigated range. The dominant change is the reduction in FF from 88.222% to 85.060%. This behaviour is consistent with the physical role of series resistance: at finite current, ohmic voltage losses increase the internal voltage drop and reduce the squareness of the J–V curve. By contrast, Voc remains almost unchanged because the net current at open circuit is approximately zero, and Jsc is only weakly affected because the device is operating at zero applied voltage.

The results are consistent with previous analyses of series resistance in PSCs. Wu et al. (2014), Kirchartz et al. (2018), and Mundhaas et al. (2019) all demonstrate that resistive losses can strongly limit fill factor and extracted power even when other photovoltaic parameters are comparatively stable.

The present numerical trend therefore agrees with the established understanding that series resistance primarily degrades the fill factor and extractable power, rather than substantially altering the open-circuit voltage or short-circuit current (Wu et al., 2014; Kirchartz et al., 2018; Mundhaas et al., 2019). In contrast, the gradual improvement obtained with increasing shunt resistance is consistent with the reduction of parasitic leakage pathways reported in previous perovskite solar-cell studies (Kirchartz et al., 2020; Tvingstedt et al., 2017). Thus, the present results provide further numerical evidence that both transport-layer doping and resistive losses must be considered together when optimizing PSC performance.

Effect of Shunt Resistance

The shunt-resistance sweep demonstrates the opposite trend. Raising Rsh suppresses parasitic leakage pathways and progressively improves FF and PCE. The results are presented in Table 4.

Table 4: Effect of Shunt Resistance on the Photovoltaic Parameters

Rsh (Ω cm²)	Voc (V)	Jsc (mA cm⁻²)	FF (%)	PCE (%)
2000	1.138294	27.21451	86.99117	26.94822
2200	1.138356	27.21451	87.14419	26.99710
2400	1.138408	27.21451	87.27172	27.03784
2600	1.138452	27.21451	87.37964	27.07232
2800	1.138490	27.21451	87.47215	27.10188
3000	1.138522	27.21451	87.55234	27.12750
3200	1.138551	27.21451	87.62250	27.14992
3400	1.138576	27.21451	87.68441	27.16970

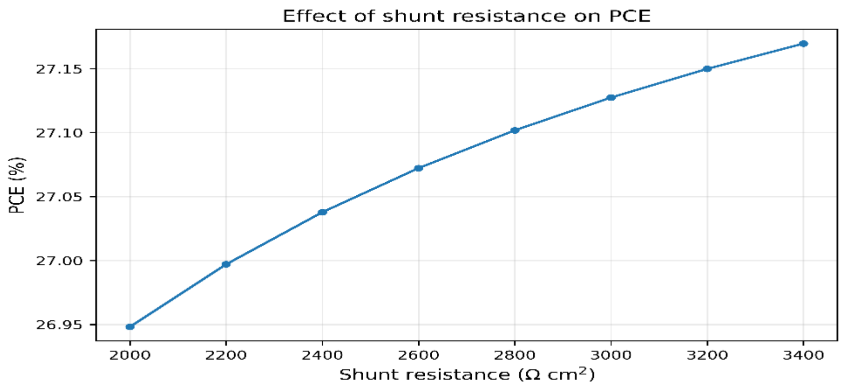

Figure 6: Effect of shunt resistance on PCE

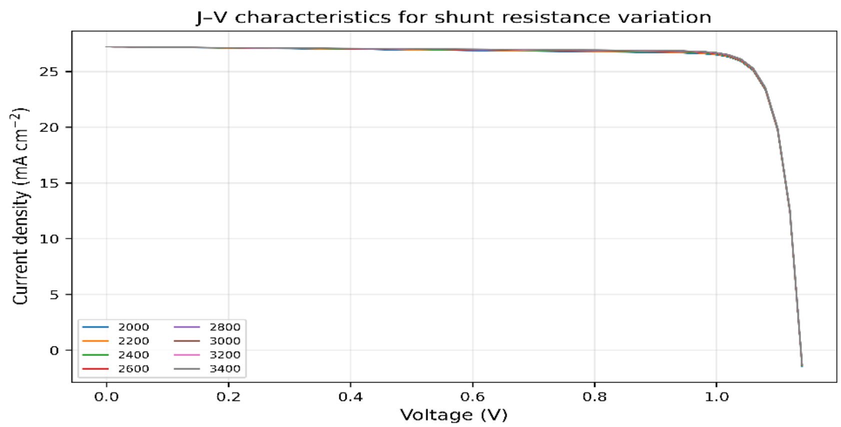

Figure 7: Simulated J–V Characteristics for Different Shunt-Resistance Values

Increasing Rsh from 2000 to 3400 Ω cm² increased FF from 86.991% to 87.684% and PCE from 26.948% to 27.170%. Jsc remained constant at 27.21451 mA cm^{-2}, while Voc increased only slightly from 1.138294 to 1.138576 V. The weak dependence of Jsc on Rsh indicates that the leakage pathway represented by the shunt resistance has little effect under short-circuit conditions within the investigated range. Its influence becomes more visible at finite voltage, where leakage currents compete with useful external current.

The gradual improvement rather than an abrupt increase in PCE indicates that the simulated device was already operating with moderately high shunt resistance. Further increases, therefore, produced diminishing gains. This behaviour agrees with the established role of shunt resistance in suppressing leakage and improving the fill factor (Kirchartz et al., 2020; Tvingstedt et al., 2017).

Integrated Optimized Device

The final optimized device reported in the MSc study combines the optimized bulk/interface defect conditions with the selected ZnSe donor concentration and resistive parameters. The integrated configuration used ZnSe donor concentration of 10^{17} cm^{-3}, Rs = 0.4 Ω cm² and Rsh = 3000 Ω cm², together with the optimized defect conditions established in the earlier stages of the work.

Table 5: Selected Photovoltaic Results Reported for the Sequential and Final Integrated Optimization

Optimization stage	Jsc (mA cm^{-2})	Voc (V)	FF (%)	PCE (%)
Initial device	27.22	1.14	88.68	27.49
Optimized bulk defects	30.89	1.23	80.01	30.39
Optimized interface defects	29.68	1.22	79.09	28.73
Optimized doping concentration	27.22	1.14	88.68	27.49
Series resistance optimization	29.67	1.22	78.29	28.44
Shunt resistance optimization	29.68	1.22	78.16	28.37
Final integrated optimization	30.89	1.23	78.29	29.70

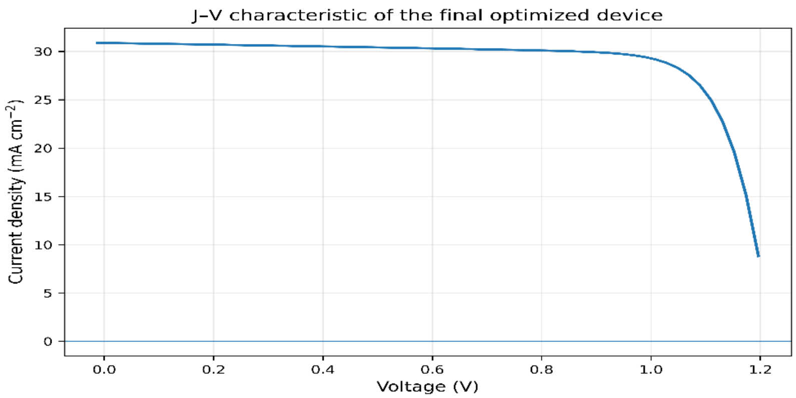

Figure 8: J–V characteristic of the final optimized device reconstructed from the SCAPS chart data embedded in the MSc thesis

The final integrated device achieved Jsc = 30.89 mA cm^{-2}, Voc = 1.23 V, FF = 78.29% and PCE = 29.70%. The increase in PCE from the initial 27.49% to 29.70% represents an absolute improvement of 2.21 percentage points. The final J–V characteristic exhibits a high photocurrent plateau and a pronounced knee before the open-circuit region, consistent with the high extracted power reported in the thesis.

The final 29.70% value should not be attributed solely to ZnSe doping or Rs/Rsh optimization because the integrated result also incorporates the preceding absorber-bulk and interface-defect optimization. The isolated resistance sweeps show that the best tested individual Rs point was 0.2 Ω cm^2, while the best tested individual Rsh point was 3400 Ω cm^2. The final integrated model instead used 0.4 Ω cm^2 and 3000 Ω cm^2 together with the other optimized parameters. This distinction is retained here to avoid conflating isolated parameter maxima with the final multivariable configuration.

CONCLUSION

SCAPS-1D numerical simulations were used to investigate the influence of ZnSe donor concentration, series resistance and shunt resistance on an FTO/ZnSe/$MASnI_3$/Graphene/Au perovskite solar cell. ZnSe donor concentration produced a pronounced non-monotonic influence on the photovoltaic response, with the optimum baseline performance obtained at 10^{17} cm^{-3}, corresponding to Voc = 1.139 V, Jsc = 27.215 mA cm^{-2}, FF = 88.675% and PCE = 27.486%. Increasing the donor concentration to 10^{19} cm^{-3} reduced the PCE to 21.586%, demonstrating that excessive doping does not necessarily improve device efficiency. Series resistance primarily affected the fill factor and PCE, with an increase from 0.2 to 1.6 Ω cm^2 reducing FF from 88.222% to 85.060% and PCE from 27.346% to 26.367%, while Voc and Jsc remained nearly unchanged. Conversely, increasing shunt resistance from 2000 to 3400 Ω cm^2 improved FF from 86.991% to 87.684% and PCE from 26.948% to 27.170%, while Jsc remained essentially constant. These results demonstrate the importance of controlled ZnSe donor doping, low series resistance and sufficiently high shunt resistance for reducing electrical losses and improving charge extraction. The final integrated configuration reported in the MSc study achieved Jsc = 30.89 mA cm^{-2}, Voc = 1.23 V, FF = 78.29% and PCE = 29.70%. However, this final value incorporates the preceding absorber bulk- and interface-defect optimization in addition to the ZnSe doping and resistive parameters; therefore, experimental validation is required to determine whether the predicted performance can be reproduced in fabricated ZnSe/$MASnI_3$/graphene devices.

REFERENCES

Ameen, S., Akhtar, M. S., Shin, H.-S., & Nazeeruddin, M. K. (2018). Charge-transporting materials for perovskite solar cells. In Advances in Inorganic Chemistry (Vol. 71, pp. 185–246). Academic Press. https://doi.org/10.1016/bs.adioch.2018.05.009

Baena, J. P. C., Steier, L., Tress, W., Saliba, M., Neutzner, S., Matsui, T., Giordano, F., Jacobsson, T. J., Kandada, A. R. S., Zakeeruddin, S. M., Petrozza, A., Abate, A., Nazeeruddin, M. K., Grätzel, M., & Hagfeldt, A. (2015). Highly efficient planar perovskite solar cells through band alignment engineering. Energy & Environmental Science, 8(10), 2928–2934. https://doi.org/10.1039/C5EE02608C

Burgelman, M., Decock, K., Khelifi, S., & Abass, A. (2014). Advanced electrical stimulation of thin film solar cells. Thin Solid Films, 535, 296–301. https://doi.org/10.1016/j.tsf.2012.10.032

Chen, Y., Liang, C., Zhao, D., Zhu, K., & Zhang, Y. (2019). Defect and doping concentration study with series and shunt resistance influence on perovskite solar cell performance: A numerical investigation. Solar Energy, 184, 420–427. https://doi.org/10.1016/j.solener.2019.04.023

Danladi, E., Danladi, I. Y., & Danladi, A. Y. (2023). Defect and doping concentration study with series and shunt resistance influence on graphene modified perovskite solar cell: A numerical investigation in SCAPS-1D framework. Journal of the Indian Chemical Society, 100(5), 101001. https://doi.org/10.1016/j.jics.2023.101001

Hima, A., Lakhdar, N., Benbrahim, S., & Bensacia, N. (2017). Numerical simulation of perovskite solar cells using SCAPS-1D: Effect of doping concentration and layer thickness. Materials Science and Engineering: B, 226, 76–82. https://doi.org/10.1016/j.mseb.2017.09.012

Jena, A. K., Kulkarni, A., & Miyasaka, T. (2019). Halide perovskite photovoltaics: Background, status, and future prospects. Chemical Reviews, 119(5), 3036–3103. https://doi.org/10.1021/acs.chemrev.8b00539

Karthick, S., Velumani, S., & Bouclé, J. (2019). Experimental and SCAPS simulated investigation of planar and mesoporous perovskite solar cells. Solar Energy, 192, 107–118. https://doi.org/10.1016/j.solener.2018.11.046

Kirchartz, T., Rau, U., & Nelson, J. (2018). The role of the series resistance in solar cells. Advanced Energy Materials, 8(23), 1800694. https://doi.org/10.1002/aenm.201800694

Kirchartz, T., Rau, U., & Nelson, J. (2020). Understanding the role of shunt resistance in solar cells. Progress in Photovoltaics: Research and Applications, 28(5), 367–378. https://doi.org/10.1002/pip.3241

Li, Q., Li, W., Li, Y., Lin, X., Wei, Z., & Chen, H. (2018). High-performance perovskite solar cells enabled by surface modification of ZnSe electron-transporting layers. ACS Applied Materials & Interfaces, 10(17), 14755–14763. https://doi.org/10.1021/acsami.8b01767

Li, Z., Wang, Z., Li, Y., Lv, Y., Yang, J., & Zhou, X. (2023). Highly efficient and stable planar perovskite solar cells based on thermally evaporated ZnSe electron-transporting layer. Advanced Energy Materials, 13(20), 2203649. https://doi.org/10.1002/aenm.202203649

Lin, L. (2020). Perovskite solar cells: Progress and challenges. Nature Reviews Materials, 5(6), 403–420. https://doi.org/10.1038/s41578-020-0194-7

Liu, J., Yang, J., & Wang, Z. (2020). Interface engineering in perovskite solar cells: A review. Materials Today Energy, 18, 100515. https://doi.org/10.1016/j.mtener.2020.100515

Minemoto, T., & Murata, M. (2015). Device modeling of perovskite solar cells based on structural similarity with thin film solar cells. Journal of Applied Physics, 118(7), 074504. https://doi.org/10.1063/1.4928017

Mundhaas, N., Yu, Z. J., Bush, K. A., Wang, H.-P., Häusele, J., Kavadiya, S., McGehee, M. D., & Holman, Z. C. (2019). Series resistance measurements of perovskite solar cells using Jsc–Voc measurements. Solar RRL, 3, 1800378. https://doi.org/10.1002/solr.201800378

Owolabi, J. A., Onimisi, M. Y., Ukwenya, J. A., Bature, A. B., & Ushiekpan, U. R. (2020). Investigating the effect of ZnSe (ETM) and Cu_2O (HTM) on absorber layer on the performance of perovskite solar cell using SCAPS-1D. American Journal of Physics and Applications, 8(1), 8–18. https://doi.org/10.11648/j.ajpa.20200801.12

Tailor, N. K., Kar, S., Mishra, A., & Satapathi, S. (2023). Doping in perovskite solar cells: A comprehensive review. Journal of Materials Chemistry C, 11(5), 1561–1582. https://doi.org/10.1039/D2TC04481K

Tvingstedt, K., Gil-Escrig, L., Momblona, C., Rieder, P., Kiermasch, D., Sessolo, M., Baumann, A., Bolink, H. J., & Dyakonov, V. (2017). Removing leakage and surface recombination in planar perovskite solar cells. ACS Energy Letters, 2(2), 424–430. https://doi.org/10.1021/acsenergylett.6b00721

Ukorah, I. N., Owolabi, A. J., Ali, H., Onimisi, M. Y., Tafida, R. A., Olalekan, A. J., Gambo, H. M., Usman, S. L., Christiana, A. O., Ukwenya, J. M., Akinade, B. J., & Ugbe, R. U. (2024). Investigating the performance of tin-based perovskite solar cell with zinc selenide as an ETM and graphene as an HTM using SCAPS-1D. Progress in Physics of Applied Materials, 4(2), 171–181. https://doi.org/10.22105/ppam.2024.445621.1085

Wu, Y., Xie, F., Chen, H., Yang, X., Su, H., Cai, M., Zhao, Z., Zhou, T., Noda, T., Han, L., & Sun, Q. (2014). Analysis of series resistance in perovskite solar cells. Advanced Materials, 26(30), 5173–5178. https://doi.org/10.1002/adma.201401487

Zarazua, I., Han, G., Boix, P. P., Mhaisalkar, S., Fabregat-Santiago, F., Mora-Seró, I., & Bisquert, J. (2016). Surface recombination and collection efficiency in perovskite solar cells from impedance analysis. The Journal of Physical Chemistry Letters, 7(24), 5105–5113. https://doi.org/10.1021/acs.jpclett.6b02193